EFFICIENT SIMULATION OF INCOMPRESSIBLE VISCOUS FLOW OVER MULTI-ELEMENT AIRFOILS

Stuart E. Rogers
N. Lyn Wiltberger
Dochan Kwak
MS 258-1, NASA Ames Research Center, Moffett Field, CA 94035

Abstract

The incompressible, viscous, turbulent flow over single and multi-element airfoils is numerically simulated in an efficient manner by solving the incompressible Navier-Stokes equations. The computer code uses the method of pseudo-compressibility with an upwind-differencing scheme for the convective fluxes, and an implicit line-relaxation solution algorithm. The motivation for this work includes interest in studying high-lift take-off and landing configurations of various aircraft. In particular, accurate computation of lift and drag at various angles of attack up to stall is desired. Two different turbulence models are tested in computing the flow over an NACA 4412 airfoil; an accurate prediction of stall is obtained. The approach used for multi-element airfoils involves the use of multiple zones of structured grids fitted to each element. Two different approaches are compared; a patched system of grids, and an overlaid Chimera system of grids. Computational results are presented for two-element, three-element, and four-element airfoil configurations. Excellent agreement with experimental surface pressure coefficients is seen. The code converges in less than 200 iterations, requiring on the order of one minute of CPU time on a CRAY YMP per element in the airfoil configuration.

Introduction

An increased understanding of high-lift systems will play an important role in designing the next generation of transport aircraft. Current designs for such aircraft typically involve multiple elements, such as leading edge slats and multiple-slotted flaps. The current trend is toward a more efficient, yet simpler design which will lead to reduced manufacturing and maintenance costs. At the same time, increases in lift coefficients for a given angle of attack and increases in maximum lift coefficient will lead to a larger payload capability. Improved designs will also allow for reduced noise in areas surrounding airports. Understanding of high-lift flow physics harbors the potential to improve airport capacity through a reduction of an airplane's wake vortices, allowing closer spacing between subsequent airplanes taking off and landing.

Increased knowledge of the flow physics involved with high-lift systems is therefore of greater interest than ever before as the need to improve over current designs becomes acute. Study of these configurations will require both computational and experimental efforts. Computational fluid dynamics (CFD) is playing a large role in this work. Multi-element configurations present a number of challenging problems to the numerical investigators. These include problems involving turbulent boundary layer separation, confluent boundary layers and wakes, Reynolds number effects, three-dimensional effects, compressibility effects, transition, and complex geometries. Although the problems are inherently three-dimensional, there is still much to be learned about the flow physics by studying two-dimensional models.

The computational tools available range from the more efficient inviscid/viscous coupled methods, to a Reynolds-averaged Navier-Stokes (RANS) analysis. An example of the former method is given by Kusunose et al.[1] They use a full potential method coupled with an integral boundary-layer method. These methods have been found to be successful in accurately computing the pressure distribution for multi-element airfoils, including cases up to maximum lift, some of which involve separation. The coupled method has been proven to be useful as an effective engineering design tool. This method is limited by its inability to compute beyond maximum lift conditions, and may have problems with certain features of some airfoil systems such as flap wells, thick trailing edges, or unsteady effects.

Navier-Stokes calculations for high-lift systems have been investigated by a number of authors.[2-4] Schuster and Birckelbaw[2] computed the flow over a two-element airfoil using a structured, compressible, RANS solver. The grid system used was a pointwise patched system with three zones, with C-grids around both the main element and flap, and another outer C-grid surrounding those. Good results were obtained for low Reynolds number turbulent flow. The next two authors, Barth,[3] and Mavriplis[4] both used an unstructured grid approach to handle the difficulty of discretizing multi-element geometries. They were each able to produce accurate pressure coefficient information on the airfoil surfaces. The accuracy of the unstructured grid approach, however, is limited because of the very large aspect ratio of the triangular cells required to resolve high Reynolds number boundary layer flows. Also, this approach is not well developed for three-dimensional problems. Large computational resources are required, especially CPU memory, to make these methods work for viscous flows. Unstructured methods are currently generating a lot of interest in the research community; improvements to these limitations are to be expected in the near future. Until such a time, the current authors believe that a structured grid approach is the most suitable for solving viscous multi-element problems in two and three dimensions.

The current work uses an incompressible RANS flow solver to compute the flow over multi-element airfoils. Two different grid approaches are used; the first approach em-

ploys the patched grids utilized in Ref. 2, and the second uses an overlaid grid approach known as the Chimera scheme.[5] The current work examines several airfoil flow problems in two dimensions in an effort to characterize current capability to numerically study such problems. Grid topology, computational efficiency, and resulting accuracy are issues to be examined in the current work. An incompressible flow solver is being utilized because the flow conditions for take-off and landing will generally be less than a Mach number of 0.2. In the actual flow, compressibility effects will generally be confined to a small localized region, such as near the area of a leading-edge slat. Since the incompressible Navier-Stokes system has one less equation than its compressible counterpart, less computing resources are required.

Algorithm

The current computations are performed using the INS2D computer code which solving the incompressible Navier-Stokes equations for steady-state flows[6] and for unsteady computations.[7] This algorithm has also been applied to problems in three dimensions using the INS3D-UP code.[8] The code is based on the method of artificial compressibility as developed by Chorin[9] in which a pseudo-time derivative of pressure is added to the continuity equation. Thus the convective part of the equations form a hyperbolic system, which can be iterated in pseudo-time until a steady-state solution is found. For unsteady problems, subiterations in pseudo-time are performed for each physical time step. Since the convective terms of the resulting equations are hyperbolic, upwind differencing can be applied to these terms. The current code uses flux-differencing splitting modeled after the scheme of Roe.[10] The upwind differencing leads to a more diagonally dominant system than does central differencing and does not require the additional use of artificial dissipation. The system of equations is solved using a Gauss-Seidel type line-relaxation scheme. The line-relaxation scheme is very useful for computing multi-zonal grids because it makes it possible to iteratively pass ΔQ (which is the change in the dependent variables for one time step) information between the zonal boundaries as the line-relaxation sweeping takes place. The result is a semi-implicit passing of boundary conditions between zones, which further enhances the code stability.[11] The resulting code is very robust and stable. It is capable of producing steady-state solutions to fine-mesh problems in 100 to 200 iterations. More detail about the computer code can be found in Refs. 6-8.

Most of the present calculations used the turbulence model developed by Baldwin and Barth,[12,13] where the specific formulation found in Ref. 12 was used. This is a one-equation turbulence model that avoids the need for an algebraic length scale and is derived from a simplified form of the standard $k-\epsilon$ model equations. In the current application, the equation is solved using a line-relaxation procedure similar to that used for the mean-flow equations. This model has been found to be very robust and easy to implement for multiple-body configurations. The next section includes computations of flow over a single airfoil. One of the studies for this problem includes a comparison of the Baldwin-Barth turbulence model with the Baldwin-Lomax[14] algebraic turbulence model.

Computed Results

NACA 4412 Airfoil

Calculations were performed for the flow over an NACA 4412 airfoil at a Reynolds number of 1.52 million. A C-grid with dimensions of 241x63 was used, with wall spacings on the order of $10,^{-5}$ which corresponds to y^+ values on the order of one. The grid was computed using a hyperbolic grid generator.[15] A close view of this grid is shown in fig. 1.1. In order to compute flow quantities for the points on the computational boundary in the "wake cut" line of the c-mesh, two lines of dummy points are added such that these dummy points coincide with points on the other side of the wake line. The first line of these dummy points is updated by injecting values from the coincident interior points on which they lie. Using this overlap produces smooth solutions to the equations across this computational boundary. This procedure also adds dummy points inside the airfoil. These points are merely blanked out and never used in the solution procedure. All of the C-grids in this work use this overlap.

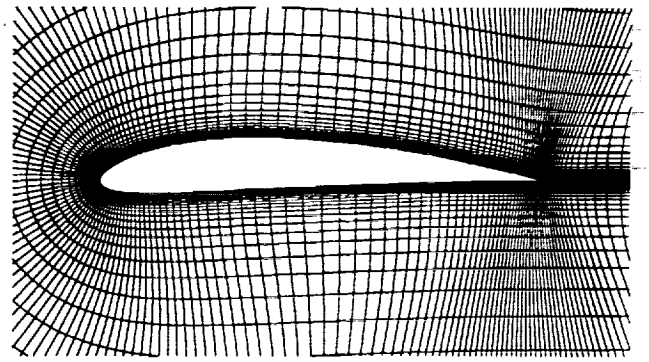

Fig. 1.1. 241x63 grid used for flow over an NACA 4412 airfoil.

This flow was computed using two different turbulence models, the Baldwin-Barth model[12] and the Baldwin-Lomax model.[14] Figure 1.2 shows a comparison between these computations and the experimental results of Coles and Wadcock[16] at an angle of attack of 13.87 degrees, which is very nearly maximum lift conditions. In the experiment the flow separated at approximately 85 percent of chord. Trip-strips were employed in the experiment on the suction and pressure surfaces at chord locations of x/c of 0.023 and 0.1, respectively. The computations thus specify these as the transition points. For the Baldwin-Barth model this is implemented by setting the the production terms to zero upstream of these locations; for the Baldwin-Lomax model the eddy viscosity is set to zero upstream of the transition location. The agreement is fairly good, with the biggest

discrepancy occurring at the trailing edge where the predicted pressure is too high. However, the Baldwin-Barth model does give a flattening of the pressure over the aft 15 percent of chord, indicating flow separation, where the Baldwin-Lomax solution does not show this tendency. This figure also shows that the computations with the transition predict a leading-edge laminar separation bubble. The experiment reports that there was no laminar separation bubble at this angle of attack, so an additional computation was run using the Baldwin-Barth model with the production terms turned on everywhere, thus the boundary layer was fully turbulent. The pressure coefficient for this is also shown in fig. 1.2. There is a slight improvement in the trailing edge area for this solution. The Baldwin-Lomax model showed no difference in the pressure or velocity solution when it was run without specifying transition, except that it removed the laminar separation bubble.

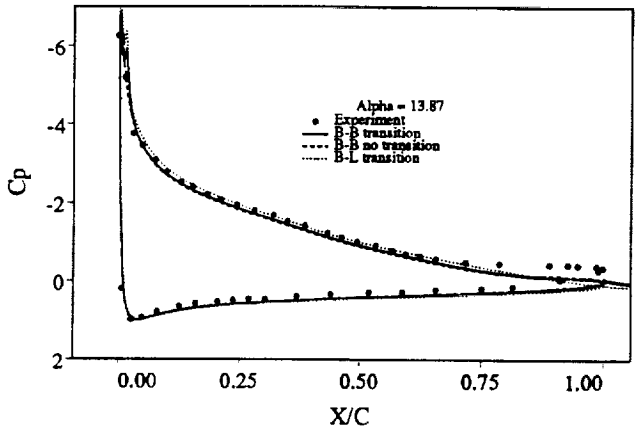

Fig. 1.2. Pressure coefficient on surface of an NACA 4412 airfoil at Reynolds number of 1.52 million comparing calculations with Baldwin-Barth and Baldwin-Lomax turbulence models and experimental data.

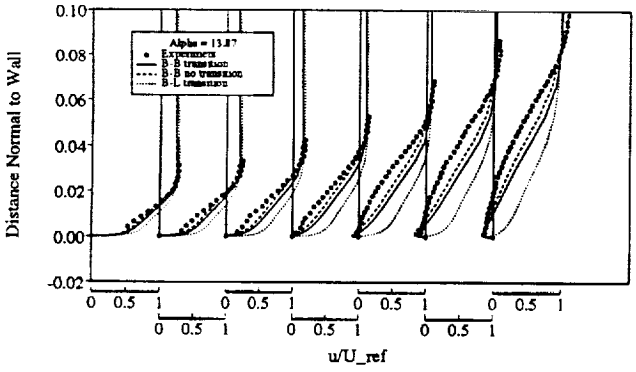

Fig. 1.3. Velocity profiles on upper surface of an NACA 4412 airfoil at streamwise stations of x/c = 0.62, 0.675, 0.731, 0.786, 0.842, 0.897, and 0.953.

Velocity profiles from the suction surface boundary layer are plotted in fig. 1.3 at streamwise stations of x/c = 0.62, 0.675, 0.731, 0.786, 0.842, 0.897, and 0.953. The profiles are shown using the streamwise component of velocity in boundary-layer coordinates, that is, the velocity component tangential to the local airfoil surface. This figure shows in greater detail the problems of the Baldwin-Lomax solutions in this region: the boundary layer profile is too full and the solution shows only a tiny region of separation. The Baldwin-Barth solution is in closer agreement with the experimental results, but also suffers from too small of a separation region. The case without transition shows the best agreement with the experimental profiles.

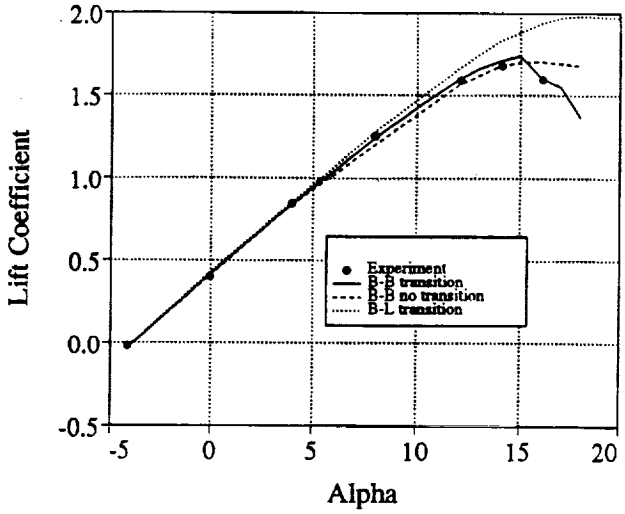

Fig. 1.4. Lift coefficient versus angle of attack for flow over an NACA 4412 airfoil.

Computations were run for a range of angles of attack from zero lift to maximum lift. The lift coefficient versus angle of attack is plotted in Fig. 1.4. This shows that the Baldwin-Barth solution with transition gives very good agreement in the lift, including the prediction of stall. For all cases, as the angle of maximum lift was approached the flow tended toward unsteadyness. That is, the steady-state computations did not converge completely, which, for the artificial compressibility formulation means that the results do not satisfy the continuity equation. In these cases the code was then run in a time-accurate, unsteady mode. For the Baldwin-Barth model with transition, at an angle of attack of 14 degrees, the unsteadiness dies out when the computations are run in a time-accurate mode. At 16 degrees, an unsteady periodic behavior ensues; as shown in the figure, the mean lift drops sharply below the values from smaller angles of attack. Examination of the flow shows that the leading-edge laminar separation bubble is periodically shedding and traveling through the boundary layer on the top surface of the airfoil, and past the trailing edge. Figure 1.5 shows the pressure coefficient on the surface of the airfoil at seven different times through the period of this flow. The forming of the leading-edge vortex is evident, and it can be seen that it travels downstream and past the trailing edge.

For the Baldwin-Barth model without transition at an angle of attack of 16 degrees, all oscillations damp out and it converges to a steady-state solution. At 18 degrees, the lift continues to oscillate periodically, yet there is only a slight

drop in the lift, and there is a complete absence of a leading-edge separation bubble. The Balwin-Lomax computations do not have any type of periodic unsteady behavior with or without transition. The results from this model show that a drop in lift does not occur until an angle of attack of 20 degrees.

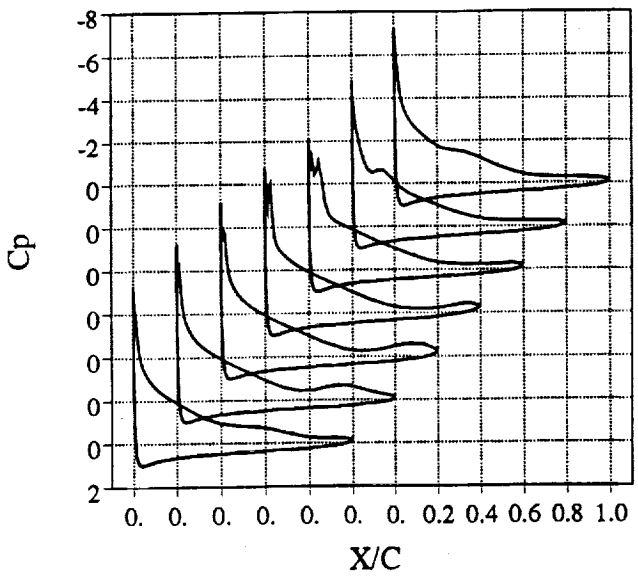

Fig. 1.5. Pressure coefficient on the surface of the NACA airfoil at 16 degrees angle of attack for seven different times during the unsteady periodic motion.

In short, the Baldwin-Barth model shows promise for use in predicting high-lift flows, and although some deficiencies are shown here, it is significantly better than the Baldwin-Lomax model. In addition, the Baldwin-Barth model is much easier to use than the Baldwin-Lomax model, in that is does not require a length scale; it is straightforward to implement for a multi-element airfoil computation. All of the results in the later sections of this paper use the Baldwin-Barth model.

The convergence history is shown in Fig. 1.6 for the angle of attack of 13.87 degrees for both turbulence models with and without transition. In general, fast convergence is seen, with converged solutions obtained in 100 to 200 iterations. Specifying the transition tends to produce an unsteady component into the flow field which somewhat delays the convergence. It can also be seen that the Baldwin-Lomax computations converge much faster than the Baldwin-Barth model. The computing time on a Cray YMP required for this 241 x 63 mesh is 100 seconds for 200 iterations when using the Baldwin-Barth model, 90 seconds for 200 iterations with the Baldwin-Lomax model. When running the unsteady cases, the algorithm requires subiterations at each physical time step to drive the divergence of velocity toward zero. When running the unsteady 16 degree angle of attack case with a non-dimensional time step of 0.05, 40 physical time steps resulted in one period of the flow. This took about 10 minutes of computing time. Due to the difficult nature of solving the unsteady incompressible Navier-Stokes equations, it proably would not be computationally cheaper to use an incompressible formulation over a compressible Navier-Stokes code to study post-stall, unsteady airfoil flows.

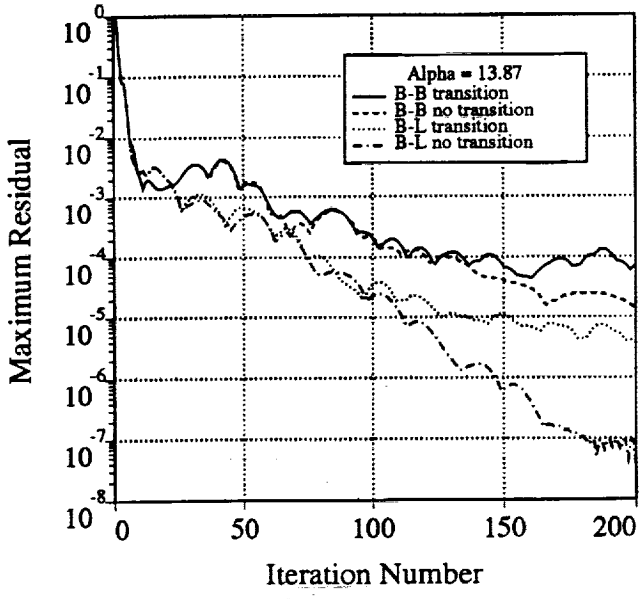

Fig. 1.6. Convergence history showing Maximum residual versus iteration number for flow over an NACA 4412 airfoil at 13.87 degrees angle of attack.

Two-Element Airfoil

The geometry is made up of an NACA 4412 airfoil with an NACA 4415 flap deployed at 21.8 degrees, with the entire configuration at 8.2 degrees angle of attack. This geometry was studied experimentally by Adair and Horne.[17] The chord Reynolds number was 1.8 million, and the Mach number in the experiment was 0.09. The blockage in the wind-tunnel was severe enough that the wind-tunnel walls needed to be included in the calculations in order to get good agreement with the experimental pressure coefficients.

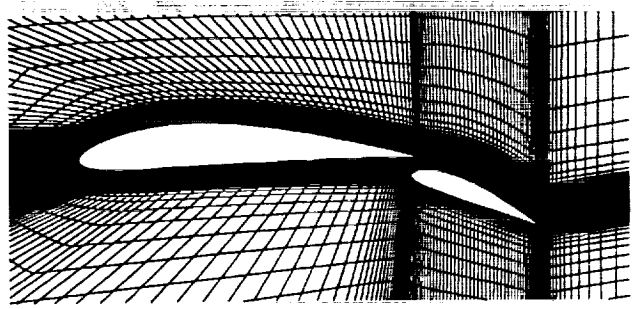

Fig. 2.1. Three-zone patched grid used to compute flow over an NACA 4412 airfoil with an NACA 4415 flap.

The airfoils were discretized using two different grid approaches. The first follows the work of Schuster and

Birckelbaw[2] and uses 3 zones which are patched together using coincident points. This grid is shown in Fig. 2.1. Each of the elements is surrounded by a C-grid, and these two grids are surrounded by another C-grid which extends out to the wind-tunnel walls. The dimension of these grids are 374x44, 241x33, and 352x32, respectively, for a total of 35,000 points.

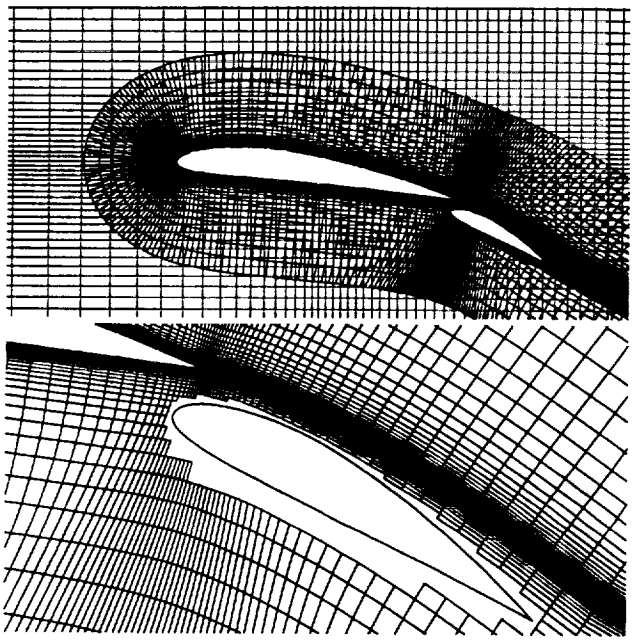

Fig. 2.2. Overlaid Chimera grid used to compute flow over an NACA 4412 airfoil with an NACA 4415 flap.

The second type of grid uses a Chimera[5] approach, in which C-grids were generated about each of the elements. To include the effects of the wind-tunnel walls these grids were inset into a third zone composed of an h-grid. A partial view of these three grids is shown at the top of Fig. 2.2, with a close-up of the main-element grid in the vicinity of the flap shown in the bottom half of this figure. These grids had dimensions of 261x49, 203x35, and 121x61, for a total of 27,500 points. To implement the Chimera approach, these grids are given to the PEGSUS[5] code. This code first punches holes into grids where they overlap a body (as shown in the bottom of Fig. 2.2). It then computes the interpolation stencils used to update the flow quantities at the fringe points of these holes, and to update the flow quantities at the outer boundaries of grids which lie inside another grid (like the outer boundaries of the c-grids seen in the top of Fig. 2.2). For both the Chimera and the patched grid approaches, the spacing next to the surfaces was set to 2×10^{-5}, which correspond to y^+ values at the wall on the order of one.

The computational results compare well with the experimental results of Adair and Horne.[17] A plot of the pressure coefficient on the surface of the elements is shown in Fig. 2.3. Results from both of the grid approaches is shown. The biggest difference between the computation and experiment is seen in the suction peak at the leading edge of the flap. The difference might be explained by a difference in the geometry between the computations and the experiment. There was an ambiguity in the way in which the flap position is defined.

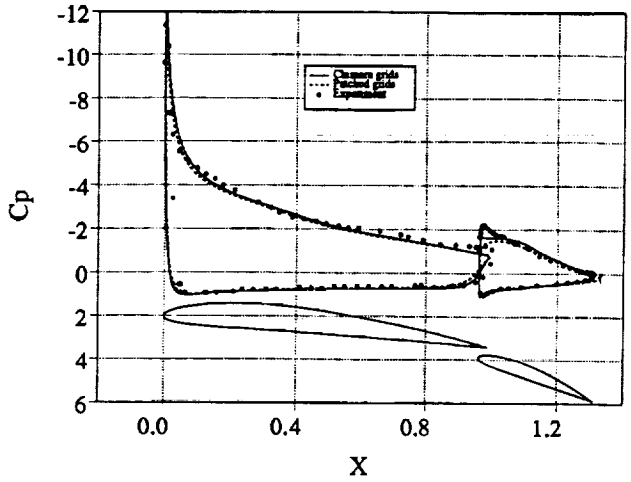

Fig. 2.3 Pressure coefficient on surface of two-element airfoil comparing both patched grid and overlaid grid schemes to experimental results.

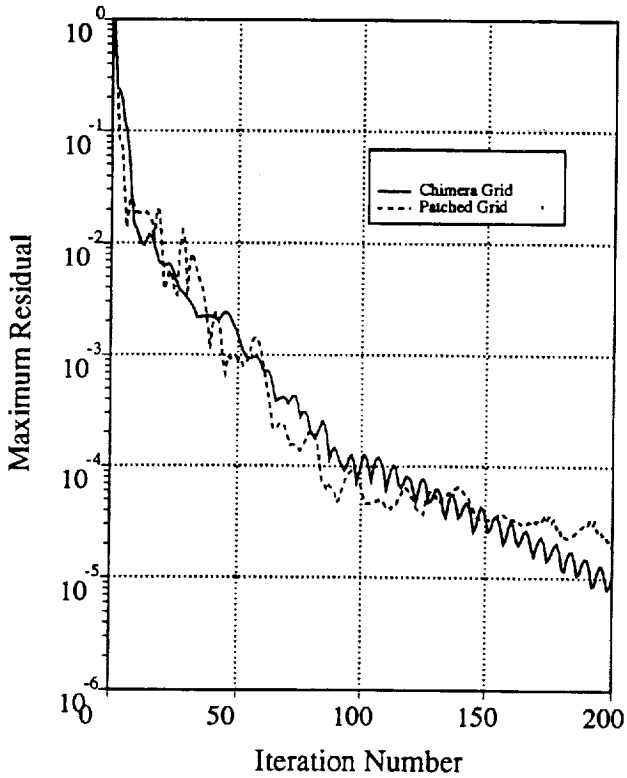

Fig. 2.4 Convergence history for flow over two-element airfoil for patched grid and overlaid grid schemes.

Figure 2.4 shows the convergence history for these computations. They both converge very well, giving a steady-

state solution in about 100 iterations. Each of these grid cases takes about 100 seconds of CPU time on a Cray YMP for 100 iterations. The code runs at about a rate of 80 MFLOPS, and requires 36 $\times 10^{-6}$ CPU seconds per grid point per iteration. Since the Chimera approach uses about 20% fewer grid points, it takes a little less computing time. The major difference between these approaches is the amount of time and effort it takes to generate the grids. The patched grid case takes on the order of several hours of work; it involves generating inner boundaries which define the surface with the proper point distribution to ensure that the grids can be patched together. Then hyperbolic grids are marched halfway across the gap from each of the elements. The resulting outer boundaries of these are merged into a common interface where they match. The inner grids are recalculated to match this interface. Finally, the outer C-grid is marched outward using a hyperbolic grid generator. The process is tedious and is not easily repeatable for a different case (new flap placement, or flap angle), or for a different geometry. On the other hand, the overlaid grids can be generated in only a matter of minutes; one need only generate two independent hyperbolic grids about each of the elements, and then feed these into the PEGSUS code[5] as described above. Once this has been set up for one case it is very easy to reproduce it for another case or another geometry. It is for these reasons that the overlaid grid approach was adopted for the rest of the cases and geometries in this work.

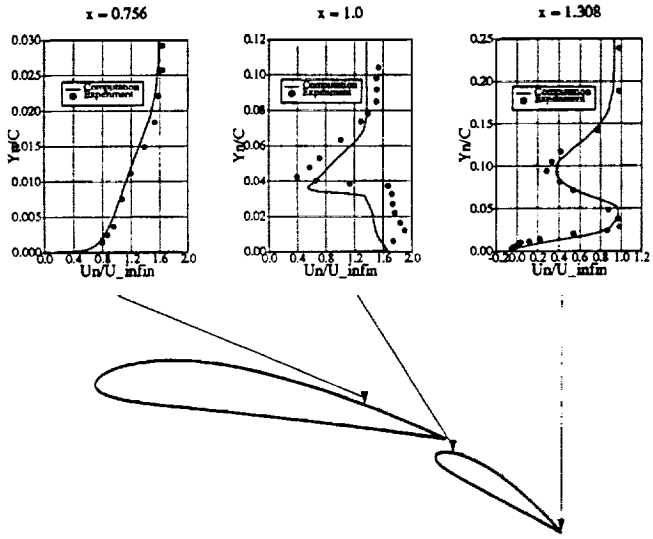

Fig. 2.5 Velocity profiles from overlaid grid calculations compared to experimental data.

Figure 2.5 shows velocity profiles from the Chimera calculations at three locations on the top surface of the main element and flap. These are plotted with experimental measurements of the profiles by Adair and Horne.[17] These plots show fairly good agreement with the experimental results. The biggest discrepancy is the difference in the gap velocity off the surface of the flap's leading edge. This is related to the difference seen in the pressure coefficient plot in Fig. 2.3. The velocity profile from the trailing edge of the flap shows that there is a separation occurring over the top surface of the flap. This profile shows that the computational separation bubble is not as thick as that seen in the experiment, but that the computations do an excellent job of capturing the wake from the main element in this region.

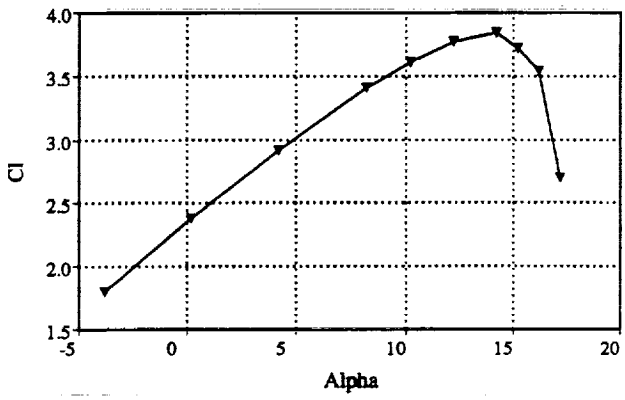

Fig. 2.6 Coefficient of lift versus angle of attack as computed by the overlaid grid approach for the two-element airfoil.

Further calculations were carried out using free-stream outer boundaries (neglecting wind-tunnel walls). These calculations use the overlaid grids with two zones, where the main element grid extends beyond ten chord lengths from the airfoil. These were run at various angles of attack to show the capability to compute maximum lift conditions as well as post-stall conditions. The curve of lift coefficient versus angle of attack is shown in Fig. 2.6. The lift drops off sharply at alpha = 15 degrees, and the calculations indicate that the flow becomes unsteady beyond that angle of attack. The skin friction along the surfaces of the airfoil elements is shown in Fig. 2.7. It can be seen that the flow separates at the trailing edge of the flap even at zero angle of attack, and that this separation reduces in size with increasing angle of attack. The main element has trailing edge separation occurring at angles of attack of 12 degrees and greater. It becomes massively separated at an angle of attack of 16 degrees. At this angle of attack the flap shows evidence of a vortex passing over the top because of the large dip in the skin friction on the surface of the flap.

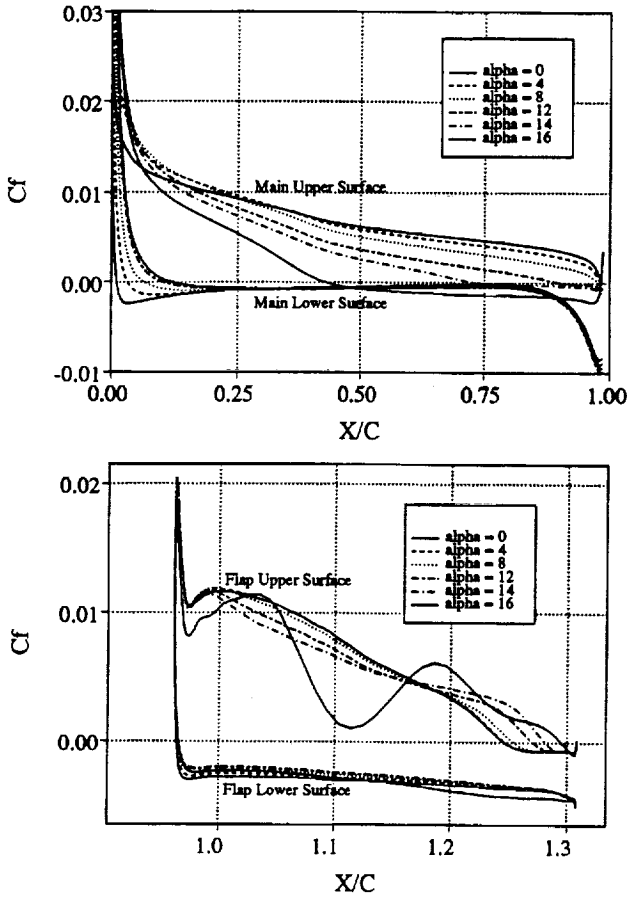

Fig. 2.7 Skin friction on the surface of the main element and flap for various angles of attack.

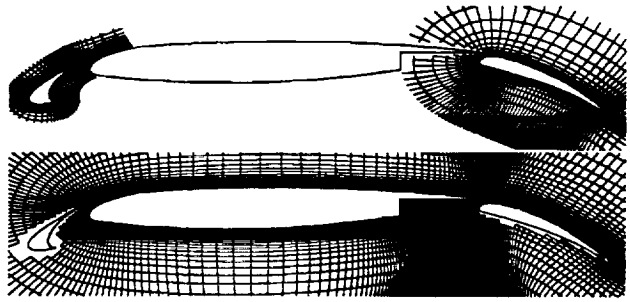

Fig. 3.1 Grid and geometry for the three-element airfoil, showing every other grid point around the slat and flap.

Fig. 3.2 Velocity magnitude contours at 20.4 degrees angle of attack.

Three-Element Airfoil

The three element computational configuration was taken from an experimental geometry of a supercritical airfoil which has been tested by Valarezo et al.[18] This airfoil consisted of a leading edge slat deployed at -30 degrees, a main element, and a trailing edge flap deployed at 30 degrees. The experimental Mach number was 0.2 and the chord Reynolds number was 9 million. The Chimera approach was used to discretize the geometry and produce a computational grid. A C-grid was placed around each element, with the main-element grid extending out to the far field. The grids for the slat-, main-, and flap-element had dimensions of 221x41, 401x75, and 221x47, respectively, for a total just under 51,000 points. The top of Fig. 3.1 shows every other grid point in the first and third element grids, with the resulting holes caused by the main element. The second half of this figure shows the main element grid. The wake cut boundary of this grid has been aligned just above the top surface of the flap element in an attempt to put as many points as possible in the wake and boundary-layer region found there.

Figure 3.2 shows velocity magnitude contours of the three element configuration run at 20.4 degrees angle of attack. The wake of the slat is clearly seen across the top of the succeeding elements. The experimental results of Valarezo et al.[18] and the computational results of this study are compared in Fig. 3.3. These figures show pressure coefficients on the surfaces of each element at three different angles of attack, 8.1, 20.4, and 23.4 degrees. Very good agreement is seen except on the suction side of the slat. Also, there is a discrepancy on the upper surface of the flap trailing edge. The experimental results show a strong adverse pressure gradient followed by a flattening in the pressure coefficient curve, which is generally evidence of flow separation. The computational results do not show this. This is probably due to the general trend of the turbulence model to underpredict the amount of separation. The experiment allowed free transition on the elements, and the computations assumed a turbulent boundary layer everywhere. Further work in this area could include use of a transition model for this calculation.

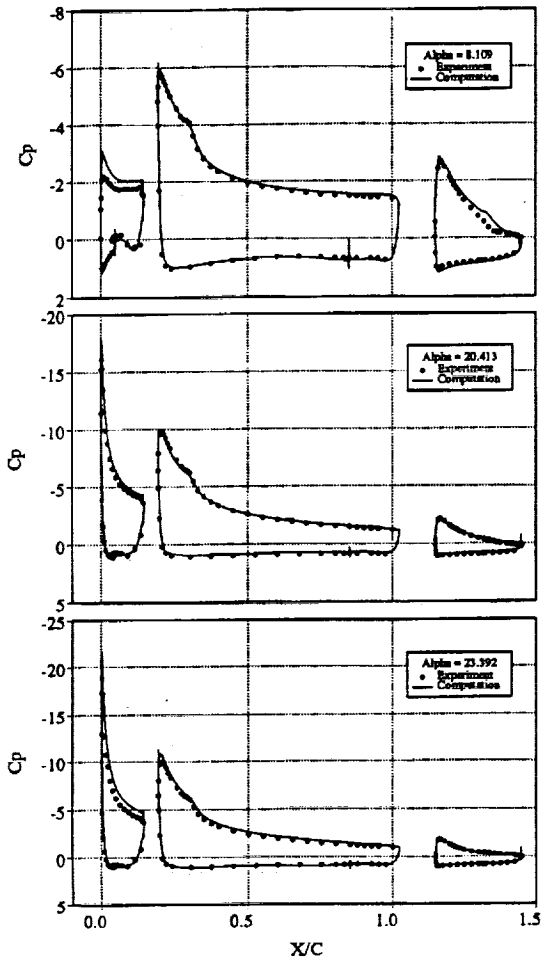

Fig. 3.3 Pressure coefficient comparing computation and experiment for angles of attack of 8.1, 20.4, and 23.4 degrees.

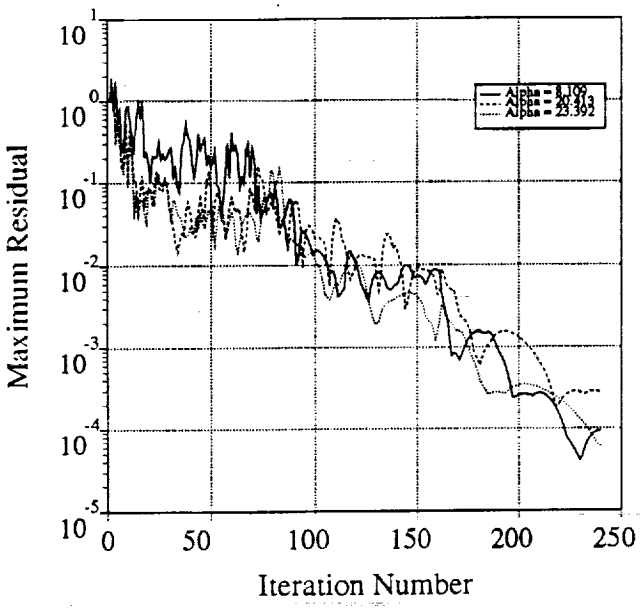

Fig. 3.4 Convergence for the three-element airfoil.

Convergence histories of these computations are shown in Figure 3.4. These computations converge well, with steady state solutions being obtained after 200 iterations, which corresponds to about 4 minutes of CPU time on a Cray YMP.

Four-Element Airfoil

The geometry is made up of a NASA 9.3 percent blunt-based, supercritical airfoil with a leading edge slat deployed at -47.2 degrees and two trailing edge flaps at 30 degree and 49.7 degrees respectively. This configuration matches the geometry used in the experimental work done by Omar et al.[19] The Mach number in the experiment was 0.201 and the chord Reynolds number was 2.83 million. The geometry was discretized using the Chimera approach. C-grids were generated around each of the elements, with the main element grid being marched out to the outer boundary. These grids were overlaid and the PEGSUS[5] code was used to create an overlaid grid. Approximately 55,000 points were used in the resulting composite grid in order to resolve the flow physics adequately in the boundary layers and wakes. The grid spacing next to the surfaces of the airfoils was 10^{-5} which ensures y^+ values of one near the wall.

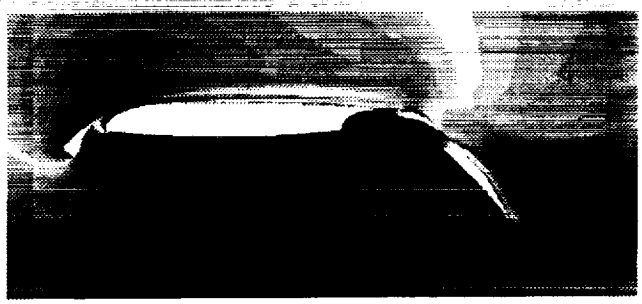

Fig. 4.1 Velocity magnitude contours at 14.25 degrees angle of attack.

The computational results of this study were compared with the the experimental results of Omar et al.[19]. Figure 4.1 shows velocity magnitude contours around the four element configuration at 14.25 degrees angle of attack. In this figure the wake from the leading edge slat is apparent over the main element. Subsequent wakes from the main element and flaps can also be observed. Plots of the pressure coefficient on the surfaces of the elements at angles of attack of 0.0, 8.13, and 14.25 degrees are shown in Fig. 4.2. Again, excellent agreement is seen except there is once more evidence that the computation of the flow over the flap underpredicts the amount of separation at the lower angles of attack.

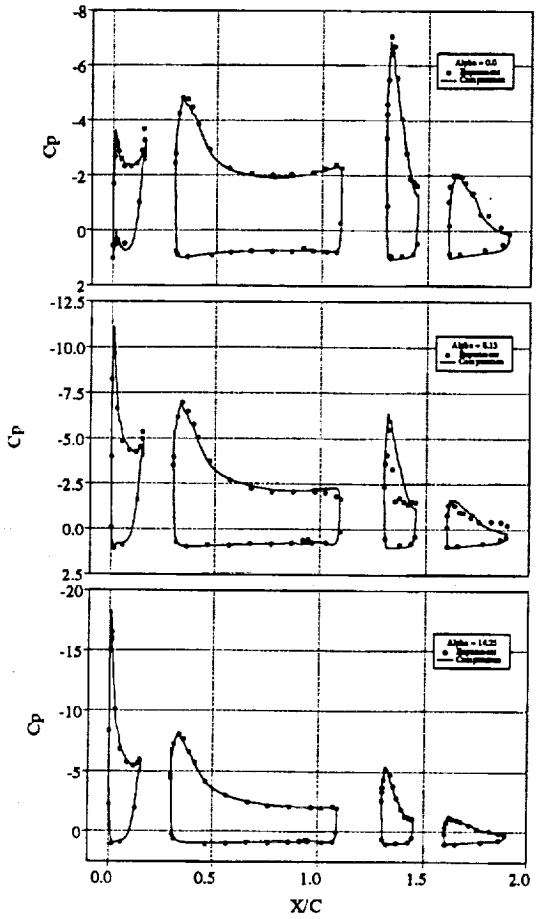

Fig. 4.2 Pressure coefficient comparing computation and experiment for angles of attack of 0.0, 8.13, and 14.25 degrees.

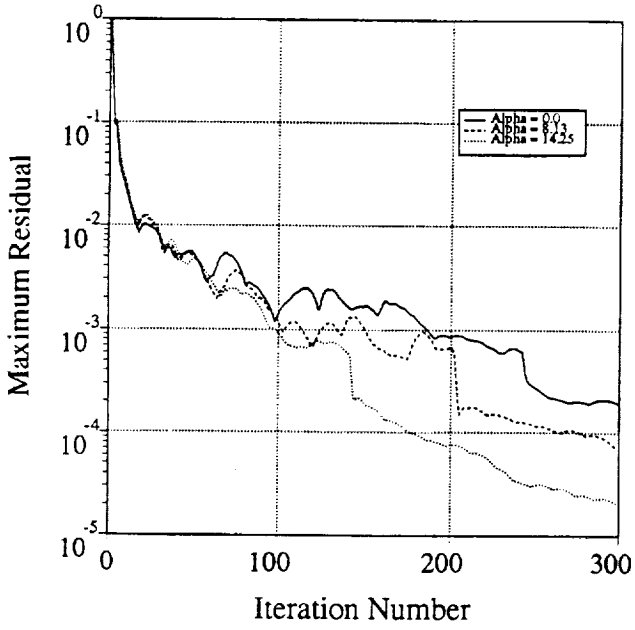

Fig. 4.3 Convergence for the four-element airfoil.

The convergence histories for the four element configuration at three different angles of attack are shown in Fig. 4.3. The computations converge well and a steady state solution is produced after about 200 iterations, which corresponds to approximately four minutes of CPU time on the Cray YMP.

Conclusions

An incompressible flow solver has been used to compute flow over several airfoil geometries for the purpose of developing a tool to study takeoff and landing configurations. The code is robust and produces numerical simulations in a matter of minutes. The flow over an NACA 4412 airfoil was investigated, and the Baldwin-Barth and Baldwin-Lomax turbulence models were compared. The Baldwin-Barth model gave significantly better results, and was much easier to use, particularly for multi-element flows. The use of the Chimera overlaid grid approach was found to be much easier than using a patched grid scheme for solving multiple element airfoil flows. Both approaches are capable of producing accurate solutions. Accurate pressure prediction was shown for geometries with two, three, and four airfoil elements. The common discrepancy between these calculations and experimental results involves separated flow. The results for the NACA 4412 airfoil indicate that deficiencies with the turbulence model are the most likely cause of these inaccuracies. Work in progress with different turbulence models shows promise in remedying this. Investigation of other turbulence models and their implementation for a multi-element airfoil calculation will be the focus of future work. In addition, future work will include the extension of the current work to three dimensions.

References

[1] Kusunose, K., Wigton, L, and Meredith, P., "A Rapidly Converging Viscous/Inviscid Coupling Code for Multi-Element Airfoil Configurations," AIAA Paper 91-0177, January, 1991.

[2] Schuster, D. M. and Birckelbaw, L. D., "Numerical Computations of Viscous Flowfields about Multiple Component Airfoils," AIAA Paper 85-0167, January, 1991.

[3] Barth, T. J., "Numerical Aspects of Computing Viscous High Reynolds Number Flows on Unstructured Meshes," AIAA Paper 91-0721, January, 1991.

[4] Mavriplis, D., "Turbulent Flow Calculations Using Unstructured and Adaptive Meshes," ICASE Report 90-61, September, 1990.

[5] Benek, J. A., Buning, P. G., and Steger, J. L., "A 3-D Chimera Grid Embedding Technique," AIAA Paper 85-1523-CP, July 1985.

[6] Rogers, S. E. and Kwak, D., "An Upwind Differencing Scheme for the Steady-state Incompressible Navier-Stokes

Equations," NASA TM 101051, November 1988. Accepted for publication in *Journal of Applied Numerical Mathematics*, to appear in 1991.

[7] Rogers, S. E. and Kwak, D., "An Upwind Differencing Scheme for the Time Accurate Incompressible Navier-Stokes Equations," AIAA Paper 88-2583, June 1988. See also *AIAA J.*, Vol. 28, No. 2, February, 1990, pp. 253–262.

[8] Rogers, S. E., Kwak, D., and Kiris, C., "Numerical Solution of the Incompressible Navier-Stokes Equations for Steady-State and Time-Dependent Problems," AIAA Paper 89-0463, January, 1989. See also *AIAA J.*, Vol. 29, No. 4, 1991, pp. 603–610.

[9] Chorin, A. J., "A Numerical Method for Solving Incompressible Viscous Flow Problems," *J. Comput. Phys.*, Vol. 2, 1967, pp. 12–26.

[10] Roe, P. L., "Approximate Riemann Solvers, Parameter Vectors, and Difference Schemes," *J. Comput. Phys.*, Vol. 43, pp. 357–372, 1981.

[11] Rogers, S. E., "On The Use of Implicit Line-Relaxation and Multi-Zonal Compuations," AIAA Technical Note 91-1611-CP, AIAA CFD Conference, Honolulu, HI, June 24-27, 1991.

[12] Baldwin, B. and Barth, T., "A One-Equation Turbulence Transport Model for High Reynolds Number Wall-Bounded Flows," NASA TM 102847, Aug. 1990.

[13] Baldwin, B. and Barth, T., "A One-Equation Turbulence Transport Model for High Reynolds Number Wall-Bounded Flows," AIAA Paper 91-0610, January, 1991.

[14] Baldwin, B. and Lomax, H., "Thin Layer Approximation and Algebraic Model for Separated Turbulent Flows," AIAA Paper 78-257, January, 1978.

[15] Cordova, J. Q. and Barth, T. J., "Grid Generation for General 2-D Regions Using Hyperbolic Equations," AIAA Paper 88-0520, January, 1988.

[16] Coles, D. and Wadcock, A. J., "Flying-Hot-Wire Study of Flow Past an NACA 4412 Airfoil at Maximum Lift," *AIAA J.*, Vol. 17, No. 4, 1979, pp. 321–329.

[17] Adair, D. and Horne, W. C., "Turbulent Separated Flow Over and Downstream of a Two-Element Airfoil," *Experiments in Fluids*, Vol. 7, pp. 531-541, 1989.

[18] Valarezo, W. O., Dominik, C. J., McGhee, R. J., Goodman, W. L., and Paschal, K. B., "Multi-Element Airfoil Optimization for Maximum Lift at High Reynolds Numbers," AIAA Paper 91-3332, September. 1991.

[19] Omar E., Zierten, T., Hahn, M., Szpiro, E., and Mahal, A., "Two-Dimensional Wind-Tunnel Tests of a NASA Supercritical Airfoil with Various High-Lift Systems," NACA CR-2215, September, 1973.